Supporting Information

Nakahara et al. 10.1073/pnas.1201628109

SI Materials and Methods

Preparation of rgs-CaM, NtCaM13, RNA Silencing Suppressor (RSS) Proteins, and Tat Peptide. Tobacco rgs-CaM cDNA was cloned between the NdeI and BamHI sites in pCold I DNA (TaKaRa) (pCold/rgs-CaM). *Escherichia coli* BL21 strain containing a chaperone plasmid pG-Tf2 was transformed with pCold/rgs-CaM. To express rgs-CaM protein, we cultured the transformant at 15 °C for 24 h in the presence of 0.5 mM isopropyl-β-D-1-thiogalactopyranoside, 1 ng mL^{-1} tetracycline, 34 μg mL^{-1} chloramphenicol, and 50 μg mL^{-1} ampicillin. His-tagged rgs-CaM protein was purified with Ni-NTA agarose (Qiagen) according to the manufacturer's instructions. RSS proteins (cucumber mosaic virus, CMV 2b, TAV 2b, TuMV HC-Pro, TBSV P19 and HIV Tat) were prepared as fusion proteins with maltose binding protein (MBP) as described previously (1). The Tat peptide associated with Tar RNA (24 aa, RKKRRQRRRPPQGSQTHQVSLSKQ) was chemically synthesized. His-tagged NtCaM13 protein was expressed using the expression vector pET16 (Merck) and purified as for rgs-CaM.

Surface Plasmon Resonance (SPR) Analysis. Physical interaction among siRNA, rgs-CaM, NtCaM13, and RSS proteins by SPR analysis were carried out as described previously (1). The rgs-CaM, NtCaM13, and RSS proteins, which were expressed in *Escherichia coli* and purified as described above, were applied to SPR analysis. The change in mass caused by the interaction between immobilized siRNAs and RSS proteins, or between immobilized rgs-CaM (or NtCaM13) and RSS proteins, which alter the refractive index of the medium, was recorded in real time through a sensorgram. The time allowed for association (sharp plateau in the line graph of the sensorgram data) and dissociation (sharp drop in the graph) phase was 60 s, respectively.

Preparation of Antibodies. Polyclonal antibodies were raised against the purified rgs-CaM protein. Anti-2b polyclonal antibodies (2), anti-ClYVV HC-Pro monoclonal antibody (3), anti-CMV capsid (CP) antibodies (Japan Plant Protection Association, Tokyo), anti-Flag M2 monoclonal antibody, anti–α/β-tubulin monoclonal antibodies (Sigma-Aldrich) and anti–green-fluorescent-protein (GFP) monoclonal antibody (Roche) were used for detection or fractionation of these proteins.

Preparation and Transfection of Tobacco BY2 Protoplasts. BY2 protoplasts were prepared and transfected with plasmids and viral transcripts as described previously (4).

Quantitative Analysis of RSS Activity in Protoplasts. RSS activity was measured using a dual-luciferase analysis in protoplasts prepared from *Nicotiana benthamiana* and *Nicotiana tabacum* leaves as previously described (1, 4). To deplete endogenous rgs-CaM, we prepared dsRNA by in vitro transcription from a PCR product amplified using the T7 promoter sequence-contained primers, 5′-GCGGGATCCTAATACGACTCACTATAGGGGCAAAAGCTCCTCTTAACTCACT-3′ and 5′-GCGGGATCCTAATACGACTCACTATAGGGGAGTACTAGTACTCTTTCTGTGAG-3′. The results are presented as means ± SD for at least three independent experiments.

Preparation of the PVX Vectors Carrying rgs-CaM and Antisense of Beclin1 cDNA. The Flag-tagged rgs-CaM ORF and the partial antisense sequence of *N. tabacum* beclin1, CTCATCCCACTCAACCGGAATTTTAGGAAGTCTTCCAAGACGAAAGTTGTTAATCGTTCCAAATTCACCATCATACCAGATTGGGAATGCATCATTGAGCACATTAGTCTTCTTTAACAGCTCTAAATGA, designed on the basis of the beclin1 homolog sequence TC145066 from the database of the Gene Index Project (http://compbio.dfci.harvard.edu/tgi/), were cloned between the ClaI and SalI sites of the PVX vector, pP2C2S (5) (PVX/Flag–rgs-CaM and PVX/asbeclin1). After linearization of these plasmids by digestion with SpeI, infectious RNAs were transcribed by T7 RNA polymerase with the Cap analog (Life Technologies) and used as inocula for mechanical inoculation.

Generation of rgs-CaM and RSSs Overexpression and Knockdown Tobacco Lines. To make a binary vector containing the rgs-CaM ORF under control of the 35S promoter, a tobacco rgs-CaM cDNA fragment amplified by PCR was cloned into the XbaI and SacI sites in pBE2113 binary (6) (pBE2113/rgs-CaM). To make an antisense–sense tandem cDNA fragment of rgs-CaM, we amplified two PCR fragments having the same rgs-CaM partial cDNA but different restriction enzyme sites with primers 5′ AAGAGTTGggatccggccggccGAATCAGTTTCTGTACCTAGTG-3′ and 5′-CCGAACCTctagagcggccgcCCTTCCATTAGTTTTGTA-3′. Both fragments were cloned in tandem into the pJM007 vector (7). The inverted repeats of rgs-CaM were cloned into the pIG121 binary vector (pIG121/IR–rgs-CaM). *Agrobacterium* EHA105 strain was transformed with pBE2113/rgs-CaM or pIG121/IR–rgs-CaM. *Agrobacterium*-mediated transformation of *N. tabacum* cv. Xanthi-nc plants was performed using leaf sections. Transgenic plants were selected on Murashige and Skoog (8) plates containing 100 μg mL^{-1} kanamycin. Transgenic tobacco plants expressing RSS proteins were also made as that overexpressing rgs-CaM. Trasgenic BY2 expressing Y2b was prepared in a previous study (9).

Agroinfiltration to Express Transgenes Transiently. RSS and GFP were transiently, simultaneously expressed in *N. tabacum* using the agroinfiltration method as previously described (10). The infiltrated area was cut out and ground for Western blotting 3 d after infiltration.

Quantitative Real-Time RT-PCR and Northern Blotting. Total RNA was extracted from leaf tissue of *N. benthamiana* or *N. tabacum* cv. Xanthi-nc and the contaminated genomic DNA was digested using TRIzol Plus RNA purification kit (Life Technologies) according to the manufacturer's manual. An endogenous mRNA level in test plants was measured by real-time PCR as described previously (11), using primers 5′-CTACATTACTCCTAAGAGTTTGAAG-3′ and 5′-ACTCATCAAAGTTGAGAACTCCATC-3′ for rgs-CaM of *N. tabacum* and 5′-TCAAATTACTCCAAAGAGTTTGAAG-3′ and 5′-ACTCATCAAAGATAAGAACTCCATC-3′ for rgs-CaM of *N. benthamiana*, which were designed on the basis of the rgs-CaM homolog sequence TC16502 from the database of the Gene Index Project (http://compbio.dfci.harvard.edu/tgi/), and 5′-agacccagattgagcaaccgttgtg-3′ and 5′-aggaagtcttccaagacgaaagttg-3′ for beclin1 of *N. tabacum*, which were designed on the basis of the beclin1 homolog sequence TC145066 from the database of the Gene Index Project (http://compbio.dfci.harvard.edu/tgi/). The results are presented as means ± SD for at least three independent experiments. Northern blotting was performed as described previously (10) using DIG-labeled cRNA probes (Roche Diagnostics). These probes were derived from the target mRNA sequences and the conserved nucleotide sequence at 3′-terminal regions of CMV genome seg-

ments. Chemiluminescent signals were quantitatively detected by LAS-4000 mini PR Lumino-image analyzer (Fujifilm).

Western Blotting. Plant tissues were homogenized in liquid nitrogen and were dissolved in 12-fold (volume/mass) denaturing buffer containing 0.125 M Tris-HCl pH 6.8, 4% (wt/vol) SDS, 10% (vol/vol) mercaptoethanol, 10% (wt/vol) sucrose, and 0.004% bromophenol blue. The extracts were boiled for 5 min and centrifuged to collect the supernatants. For detection of the rgs-CaM protein in Fig. 3 and Fig. S8, grounded tissue samples were dissolved in 12-fold (volume/mass) urea-denaturing buffer containing 4.5 M urea, 1% (vol/vol) Triton X-100, 0.5% DTT, 0.0625 M Tris-HCl pH 6.8, 2% (wt/vol) SDS, 5% mercaptoethanol, 5% sucrose, 0.002% bromophenol blue because the dissolution with the urea-denaturing buffer drastically improved the detection of the rgs-CaM protein (Fig. S8). Equal amounts of samples were separated by SDS/PAGE. Proteins were then transferred to Immobilon PVDF membranes (Millipore), and the blots were probed with antibodies. Proteins were visualized using antimouse or -rabbit secondary antibodies conjugated to alkaline phosphatase, followed by treatment either with CDP-star solutions (Roche) for chemiluminescent detection or with nitroblue tetrazolium (NBT) and 5-bromo-4-chloro-3-indolyl-phosphate (BCIP) for colorimetric detection. Chemiluminescent signals were quantitatively detected by LAS-4000 mini PR Lumino-image analyzer (Fujifilm).

Immunoprecipitation. Immunoprecipitation was carried out using Dynabeads protein G basically according to the manufacturer's manual. Fifty microliters of Dynabeads protein G was gently mixed with 5 μL of anti-Flag M2 monoclonal antibody (Sigma-Aldrich; F3165, 4.8 mg/mL) and incubated for 30 min at room temperature. The beads complex was precipitated with the magnet and washed. Viral infected leaves (0.5 g) were crushed with liquid nitrogen and dissolved in 1.5 mL PBS-1% (vol/vol) nonidet P40. The crude extract was placed into a tube containing the Dynabeads anti-Flag IgG complex and incubated with tilting and rotation for 1 h at 2–8 °C. The tube was placed on the magnet for 2 min to collect the beads and wash the complex three times in 1 mL PBS-nonidet P40 with the use of a magnet. The remaining complex was analyzed by Western blotting.

Treatment of a Tobacco Leaf with Inhibitors of 26S Proteasome and Autophagy. PBS containing 40 μM of MG132 (Sigma-Aldrich) and 20 μM of clastolactacystin β-lactone (Sigma-Aldrich) for inhibition of 26S proteasome, 5 mM of 3-methyladenine (Sigma-Aldrich), and E64-d (Sigma-Aldrich) for inhibition of autophagy or 0.2% DMSO (control) were infiltrated into a detached tobacco leaf using a 1-mL syringe. After incubation in a moist Petri dish with PBS containing inhibitors for 16 h, leaves were homogenized for Northern and Western blottings.

Immunohistochemical Studies with Tobacco BY2 Cultured Cells. Tobacco BY2 cultured cells were transformed with the Y2b gene followed by a 35S promoter (the cell line is referred to as Y2b–BY2) as described previously (9). Sucrose starvation, treatment with chemicals, and fixation of BY2 and Y2b–BY2 cells were performed as described previously (12). To detect an endogenous rgs-CaM, Y2b, and α/β-tubulin, the fixed cells were immunofluorescently stained with their specific primary, CF594 goat antirabbit IgG and CF555 rabbit antimouse IgG secondary antibodies (Biotium). These cells were also fluorescently stained with LysoTracker Green DND-26 (Life Technologies) and 4′,6-diamino-2-phenylindole (DAPI) to detect autolysosome and nuclei. Photomicrographs were taken using a Leica DMI6000 B microscope (Leica Microsystems). Image colors were then reassigned using AF6000 ver 1.5 software.

***Drosophila* S2 Cell Culturing and Examination of RSS Activity of rgs-CaM in Cells.** Tobacco rgs-CaM ORF cDNA and S6 protein gene of *Rice dwarf virus* WM variant (13) (S6wm) were cloned into pMT/V5-his (Life Technologies). *Drosophila* S2 cells stably containing rgs-CaM and S6wm genes that are under the control of metallothionein (MT) promoter were prepared by culturing cells with 300 ng mL^{-1} hygromycin after transfection with the constructed pMT plasmids. Two days after induction of the integrated rgs-CaM and S6wm genes by culturing cells in the presence of 0.5 mM Cu_3SO_4, the cells were additionally transfected with plasmids containing *Pp* and *Renilla* luciferase genes (pBie/Fluc; ref. 14, and pRL-SV40; Promega) with/without dsRNAs or siRNAs homologous to the *Pp*-luc gene. RNA silencing (RNAi) efficiency against the *Pp*-luc gene was measured with a Dual Luciferase Reporter Assay system (Promega). The results are presented as means ± SD.

Molecular Modeling, Electrostatic Potential Surface Calculation, and Docking Simulation. A homology model for the rgs-CAM protein was constructed on the basis of the crystal structure of calcium-saturated *Paramecium tetraurelia* calmodulin (PDB code: 1CLM) (15). After 100 models of rgs-CAM structure were generated using the automodel class in the program MODELER 9v6 (16), a model was chosen by a combination of the MODELER objective function value and the discrete optimized protein energy (DOPE) statistical potential score (17). The model was then refined by energy minimization (EM) with the minimization protocols in the program Discovery Studio 2.1 (Accelrys) using a CHARMm force field. Steepest descent followed by conjugate gradient minimizations was carried out until the root mean square (rms) gradient was less than or equal to 0.01 kcal mol^{-1} $Å^{-1}$. The generalized Born implicit solvent model (18, 19) was used to model the effects of solvation. The model of Angola GP was finally evaluated using the programs PROCHECK (20), WHATCHECK (21), and VERIFY-3D (22).

In addition to rgs-CaM, the crystal structure of TAV 2b was previously studied (23), and the information (PDB code: 2ZI0) was used for the following calculations. The electrostatic potential (ESP) surfaces were calculated by Delphi (24). The dielectric constants of 80 and 2 were used for the solvent and the protein, respectively, and the ESP surface for the contours from −2 kT/e (red) to +2 kT/e (blue) were visualized. Docking simulation between rgs-CaM and TAV 2b was carried out using the ZDOCK program. All figures are shown as a solvent-accessible surface representation prepared with the PyMOL Molecular Graphics system (DeLano Scientific).

1. Shimura H, et al. (2008) A strategy for screening an inhibitor of viral silencing suppressors, which attenuates symptom development of plant viruses. *FEBS Lett* 582: 4047–4052.
2. Goto K, Kobori T, Kosaka Y, Natsuaki T, Masuta C (2007) Characterization of silencing suppressor 2b of *cucumber mosaic virus* based on examination of its small RNA-binding abilities. *Plant Cell Physiol* 48:1050–1060.
3. Yambao ML, Masuta C, Nakahara K, Uyeda I (2003) The central and C-terminal domains of VPg of *Clover yellow vein virus* are important for VPg-HCPro and VPg-VPg interactions. *J Gen Virol* 84:2861–2869.
4. Shimura H, Kogure Y, Goto K, Masuta C (2008) Degree of RNA silencing and the ability of a viral suppressor vary depending on the cell species in a protoplast system. *J Gen Plant Pathol* 74:326–330.
5. Baulcombe DC, Chapman S, Santa Cruz S (1995) Jellyfish green fluorescent protein as a reporter for virus infections. *Plant J* 7:1045–1053.
6. Mitsuhara I, et al. (1996) Efficient promoter cassettes for enhanced expression of foreign genes in dicotyledonous and monocotyledonous plants. *Plant Cell Physiol* 37: 49–59.
7. Schattat MH, Klosgen RB, Marques JP (2004) A novel vector for efficient gene silencing in plants. *Plant Mol Biol Rep* 22:145–153.
8. Murashige T, Skoog F (1962) A revised medium for rapid growth and bioassays with tobacco tissue cultures. *Physiol Plant* 15:473–497.
9. Kanazawa A, et al. (2011) Virus-mediated efficient induction of epigenetic modifications of endogenous genes with phenotypic changes in plants. *Plant J* 65: 156–168.

10. Yambao MLM, et al. (2008) Point mutations in helper component protease of clover yellow vein virus are associated with the attenuation of RNA-silencing suppression activity and symptom expression in broad bean. *Arch Virol* 153:105–115.
11. Atsumi G, Kagaya U, Kitazawa H, Nakahara KS, Uyeda I (2009) Activation of the salicylic acid signaling pathway enhances *Clover yellow vein virus* virulence in susceptible pea cultivars. *Mol Plant Microbe Interact* 22:166–175.
12. Takatsuka C, Inoue Y, Matsuoka K, Moriyasu Y (2004) 3-methyladenine inhibits autophagy in tobacco culture cells under sucrose starvation conditions. *Plant Cell Physiol* 45:265–274.
13. Ando Y, Uyeda I, Murao K, Kimura I (1996) Naturally occurring phenotypic variants differing in symptom severity of rice dwarf Phytoreovirus. *Ann Phytopathological Soc Jpn* 62:466–471.
14. Matsuyama T, Asano S, Sahara K, Bando H (2003) Functional analysis of an immediate early gene, ie1, of *Bombyx mori* nucleopolyhedrovirus in mammalian cells. *J Insect Biotechnol Sericology* 72:87–94.
15. Rao ST, et al. (1993) Structure of *Paramecium tetraurelia* calmodulin at 1.8 A resolution. *Protein Sci* 2:436–447.
16. Sali A, Blundell TL (1993) Comparative protein modelling by satisfaction of spatial restraints. *J Mol Biol* 234:779–815.
17. Shen MY, Sali A (2006) Statistical potential for assessment and prediction of protein structures. *Protein Sci* 15:2507–2524.
18. Still WC, Tempczyk A, Hawley RC, Hendrickson T (1990) Semianalytical treatment of solvation for molecular mechanics and dynamics. *J Am Chem Soc* 112:6127–6129.
19. Tsui V, Case DA (2000-2001) Theory and applications of the generalized Born solvation model in macromolecular simulations. *Biopolymers* 56:275–291.
20. Laskowski RA, Macarthur MW, Moss DS, Thornton JM (1993) Procheck - a program to check the stereochemical quality of protein structures. *J Appl Cryst* 26:283–291.
21. Hooft RWW, Sander C, Scharf M, Vriend G (1996) The PDBFINDER database: A summary of PDB, DSSP and HSSP information with added value. *Comput Appl Biosci* 12:525–529.
22. Eisenberg D, Lüthy R, Bowie JU (1997) VERIFY3D: Assessment of protein models with three-dimensional profiles. *Methods Enzymol* 277:396–404.
23. Chen HY, Yang J, Lin C, Yuan YA (2008) Structural basis for RNA-silencing suppression by *Tomato aspermy virus* protein 2b. *EMBO Rep* 9:754–760.
24. Rocchia W, et al. (2002) Rapid grid-based construction of the molecular surface and the use of induced surface charge to calculate reaction field energies: applications to the molecular systems and geometric objects. *J Comput Chem* 23: 128–137.

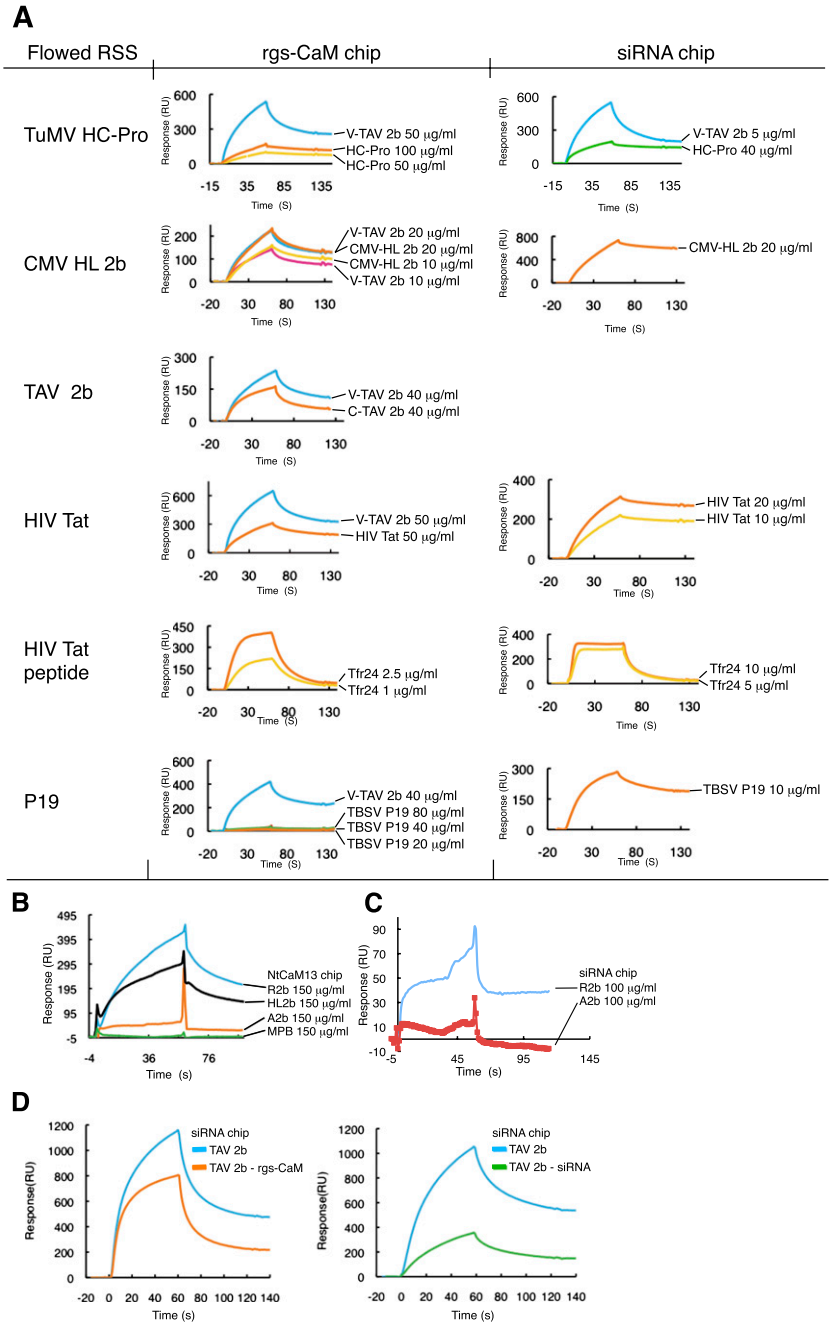

Fig. S1. Analysis of interactions of rgs-CaM and siRNA with viral RSSs using Biacore × the BIAevaluation 3.1 program. (*A*) Purified recombinant, His-tagged rgs-CaM protein, and 5′ biotin-labeled siRNA were immobilized onto sensor chips. The purified recombinant MBP–RSS fusion proteins and the Tat peptide were passed over the rgs-CaM– or siRNA-coated surface of the chip, and the change in mass due to the interaction of the immobilized rgs-CaM or siRNA with RSS proteins or the Tat peptide altered the refractive index of the medium and was recorded in real time in a sensogram. The sensogram data were corrected for nonspecific binding on the basis of the data obtained using a BSA-coated control chip. The results are summarized in Fig. 1*A*. V-TAV 2b was used as control for analysis of the interaction between rgs-CaM and RSS proteins. (*B*) Interaction of tobacco calmodulin NtCaM13 with MBP–CMV 2b fusion proteins. The recombinant His-tagged NtCaM13 protein was immobilized on a sensor chip. NtCaM13 interacted with R2b and HL2b but barely interacted with A2b and not at all with MBP. (*C*) Interaction of MBP–CMV 2b fusion proteins with siRNA. The immobilized siRNA interacted with R2b but barely with A2b. (*D*) The rgs-CaM association negatively affects the affinity of V-TAV 2b for binding siRNA as detected by SPR (*Upper* graph). As a control, the affinity of preassociated siRNA-2b to siRNA was tested. Interactions between V-TAV 2b (20 g/mL) and the siRNA immobilized on chip, the preassociates of V-TAV 2b (20 g/mL)–rgs-CaM (20 g/mL) and the siRNA on chip; V-TAV 2b (10 g/mL) and the siRNA on chip, and the preassociates of V-TAV 2b (10 g/mL)–siRNA (0.1 M) and the siRNA on chip were tested.

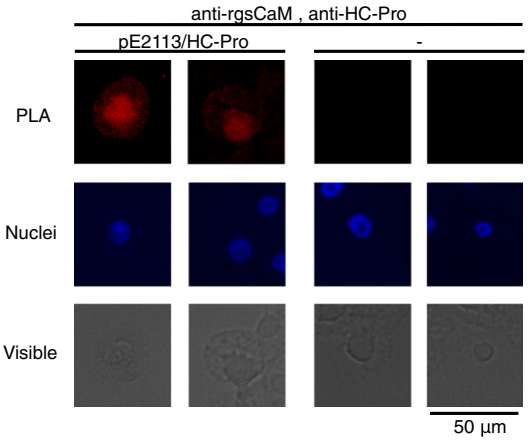

Fig. S2. In situ detection of interactions of rgs-CaM with HC-Pro. Interactions between transiently expressed ClYVV HC-Pro and endogenous rgs-CaM was detected in the proximity ligation assay (PLA) as fluorescent signals in BY2 cells. The PLA signal was shown in cells expressing HC-Pro, meaning interactions between rgs-CaM and HC-Pro. Hoechst 33342-stained nuclei (*Middle*) and merged images (*Bottom*) are also shown. (Scale bar, 50 μm.)

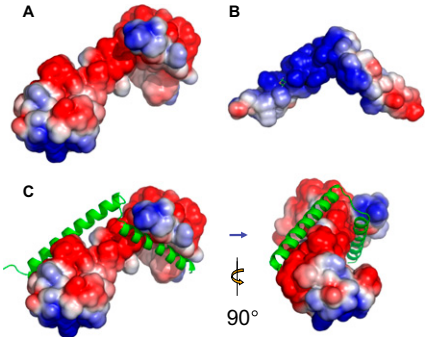

Fig. S3. Calculated surface potential on rgs-CaM and TAV 2b and docking simulation between the two proteins. Homology models of rgs-CaM (*A*) and TAV 2b (*B*) monomers were shown with the surface potential at neutral pH, with positive-charge density in blue and negative-charge density in red. (*C*) Docking simulation between rgs-CaM and TAV 2b (*Left*) and the corresponding side view (*Right*) are shown. TAV 2b is depicted as a coiled, green ribbon. One of the models with the highest scores calculated by the ZDOCK program among the top 2,000 putative rgs-CaM–TAV 2b binding configurations is shown as an appropriate example, although there are other similar structures with slight modifications.

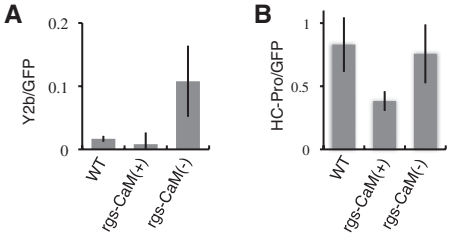

Fig. S4. (*A* and *B*) The accumulation of the RSS proteins (Y2b and HC-Pro) relative to green fluorescent proteins (GFP) in Fig. 3 *D* and *E* in bar graphs. Bars indicate SD. When the Y2b RSS and GFP were transiently and simultaneously expressed by agroinfiltration into rgs-CaM(–) and nontransgenic plants, Y2b accumulated more in rgs-CaM(–) plants than those in nontransgenic ones compared with the control GFP. However, Y2b was not detected in rgs-CaM(+) plants. It is noteworthy that the level of ClYVV HC-Pro was relatively reduced in rgs-CaM(+) plants, but we were not able to identify any significant increase in HC-Pro accumulation in rgs-CaM(–).

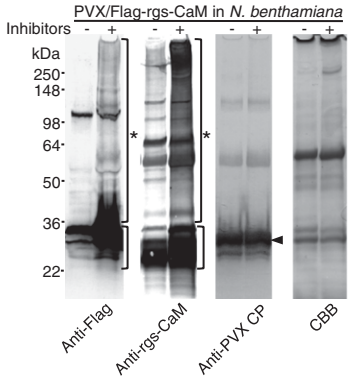

Fig. S5. Ubiquitination of rgs-CaM and its degradation dependent on 26S proteasome. Treatment of PVX/Flag–rgs-CaM–infected tobacco leaves with proteasome inhibitors (40 μM of MG132 and 20 μM of clastolactacystin-β-lactone) overnight stabilized Flag–rgs-CaM (highlighted by slanted line). A series of larger polypeptides, likely corresponding to polyubiquitinated Flag–rgs-CaM, was also detected in the sample treated with the inhibitors (the region marked by slanted line with asterisk). The inhibitors did not affect PVX CP level, noted by arrowhead. CBB-stained gels are shown as a loading control.

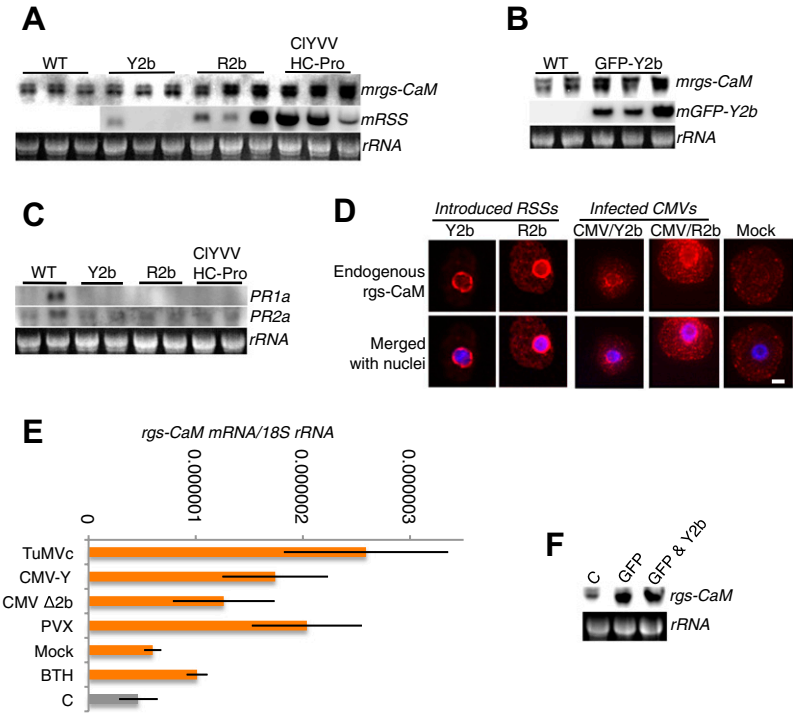

Fig. S6. (*A* and *B*) Endogenous rgs-CaM expression was induced by RSSs expressed in transgenic plants. (*C*) Induction was not due to activation of defense pathways generally because the pathogenesis-related (PR) proteins examined here were not induced. (*D*) Endogenous rgs-CaM protein was detected in situ by single recognition PLA in BY2 cells 16 h after transfection with either of the viruses (CMV/Y2b or R2b) or plasmids (Y2b or R2b). Images merged with those of nuclei stained with Hoechst 33342 (*Lower*) are also shown. Similar images representing abundance and distribution of endogenous rgs-CaM were observed in the cells of both CMV infection and transient expression of 2b, indicating induction of rgs-CaM expression at protein level by RSSs, CMV 2b, and CMV infection. (Scale bar, 10 μm.) (*E*) rgs-CaM was generally induced by viral infection, even by CMV lacking RSS, 2b (CMV Δ2b). Benzo(1,2,3)thiadiazole-7-carbothioic acid *S*-methyl ester (BTH), an analog of salicylic acid and general activator of plant defense, also weakly induced the gene. Level of mRNA of the endogenous rgs-CaM gene was detected in RNA extracts of leaves from two to four plants of *N. benthamiana* 9 d after inoculation with one of four viruses, mock inoculation (mock), treatment with salicylic acid analog (benzo-1,2,3-thiadiazole-7-carbothioic acid S-methyl ester, BTH) or untreated (control, C). Accumulation of rgs-CaM mRNA relative to 18S ribosomal RNA, as determined by real-time PCR, is shown with bars of SD. (*F*) rgs-CaM was induced simply by *Agrobacterium* infection. GFP and GFP plus Y2b RNA samples were extracts from tobacco leaves infiltrated with *Agrobacterium* transformed with the Y2b and/or GFP expression vectors. Control (C) was from a noninfiltrated leaf.

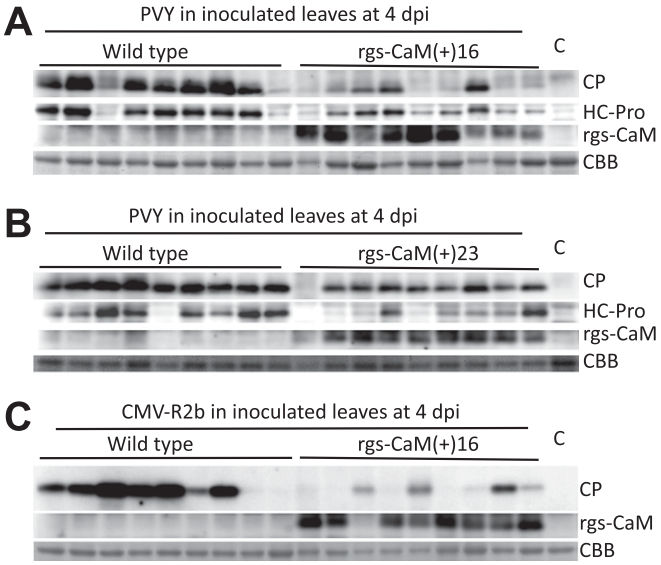

Fig. S7. (*A*–*C*) Enhanced resistance against viral infections was observed in transgenic BY tobacco plants overexpressing rgs-CaM [rgs-CaM(+)16 and 23]. Lane control (C) is sample from a healthy nontransgenic tobacco leaf.

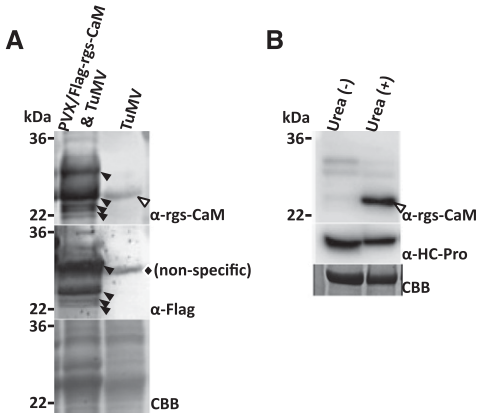

Fig. S8. (*A*) Identification of the rgs-CaM proteins by Western blotting. *N. benthamiana* was infected with PVX/Flag–rgs-CaM and/or TuMV, and extracts were derived 7 d postinfection. Western blots were performed using anti–rgs-CaM (*Top*) and anti-Flag antibodies (*Middle*). Bands that are marked by filled arrowheads were detected by both anti–rgs-CaM and Flag antibodies, suggesting that all these bands are the Flag–rgs-CaM proteins expressed by the PVX vector. The difference in migration among these bands appears to be due to modifications of the rgs-CaM proteins, including its ubiquitination. Therefore, the anti–rgs-CaM antibodies would specifically bind to rgs-CaM. However, probably because of the rgs-CaM modifications, rgs-CaM was not detected as a single band using the antibodies. The faint band marked by an open arrowhead is probably the endogenous rgs-CaM protein (rgs-CaM of *N. benthamiana*: MW 22407). A Coomassie brilliant blue (CBB)-stained gel is shown as a loading control (*Bottom*). (*B*) Improvement in detection of endogenous rgs-CaM by Western blotting using urea. We found that even endogenous rgs-CaM (rgs-CaM: MW 21059) was clearly detected as a single band by dissolving a ground leaf of the transgenic tobacco expressing ClYVV HC-Pro in the buffer containing 4.5 M Urea. Endogenous rgs-CaM proteins were detected by Western blotting with this improved procedure in Fig. 3*A*. On the other hand, urea did not affect the detection of other proteins, including ClYVV HC-Pro. CBB-stained gels are shown as loading control.

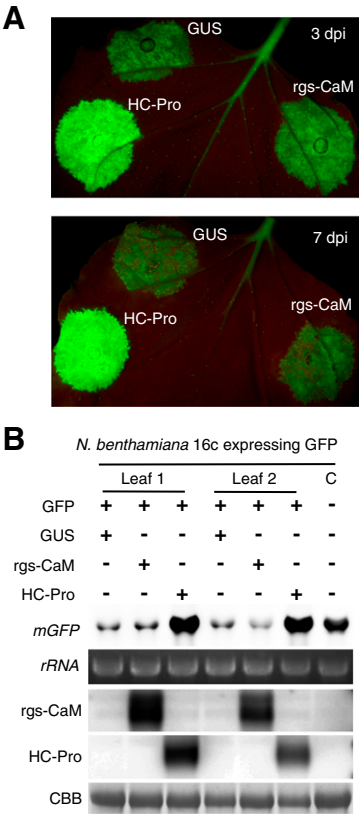

Fig. S9. RSS activity of rgs-CaM was examined by typical agroinfiltration assay with GFP-expressing transgenic *N. benthamiana* 16c. No RSS activity of rgs-CaM was detected. GFP and ClYVV P1/HC-Pro, tobacco rgs-CaM, or GUS genes were transiently expressed to trigger RNAi against GFP in 16c. RSS activity was compared on the basis of GFP fluorescence (*A*) and accumulation of GFP mRNA (*mGFP*, *B*) 3 d after infiltration. rgs-CaM and HC-Pro expression were confirmed by Western blotting.

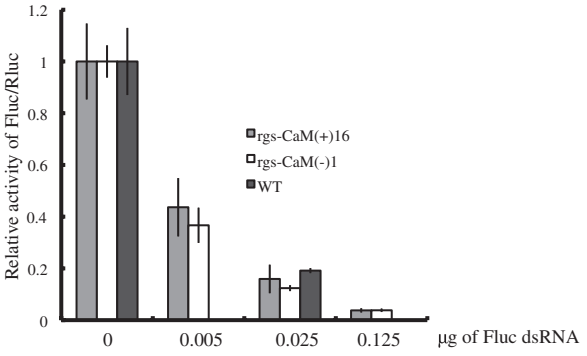

Fig. S10. Comparison of RNAi activity among protoplasts from transgenic tobacco plants, in which rgs-CaM was overexpressed [rgs-CaM(+)16] or knocked down [rgs-CaM(−)1], and wild-type plant (WT) by dual luciferase assay. Transgenic tobacco protoplasts were trasfected with the plasmids expressing luciferase proteins (Fluc and Rluc) and 0–0.125 μg of dsRNA of Fluc. The protoplast of WT was transfected with 0 and 0.025 μg of Fluc dsRNA. There was no significant difference in RNAi activity between protoplasts from transgenic tobacco plants.

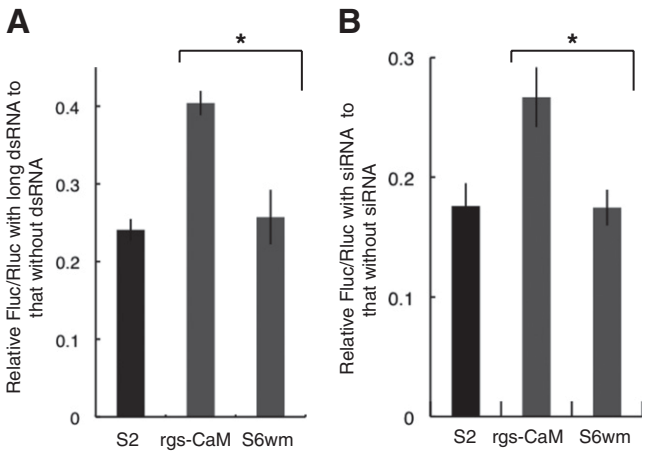

Fig. S11. Heterologous expression of tobacco rgs-CaM in S2 cells of *Drosophila melanogaster* shows that suppression of RNAi induced by both long dsRNA and siRNA. (*A* and *B*) *Pp* and *Renilla* luciferase genes (FLuc and RLuc) with/without dsRNA cognate to FLuc were used to transfect S2 cell lines, which possess the gene for tobacco rgs-CaM or *Rice dwarf virus* S6wm protein under control of the metallothionein promoter 2 d after Cu_3SO_4 induction of rgs-CaM or RDV S6wm. To normalize for differences in transfection efficiency, the transiently expressed FLuc value was normalized with that of RLuc by dual-luciferase assays 2 d after transfection. Values are FLuc intensities with dsRNA relative to those without dsRNA (*A*) and those with and without siRNA (*B*). RNAi of FLuc by both dsRNA and siRNA were significantly attenuated in the S2 cell line expressing rgs-CaM but not in the line expressing RDV S6wm or original S2 cells (*$P < 0.01$ versus controls; paired Student *t* test), suggesting that rgs-CaM interferes at a step of RNAi after siRNA production.